AJNR

Cerebral Damage after Carbon Monoxide Poisoning: A Longitudinal Diffusional Kurtosis Imaging Study

Y. Zhang, T. Wang, J. Lei, S. Guo, S. Wang, Y. Gu, S. Wang, Y. Dou and X. Zhuang

Cerebral Damage after Carbon Monoxide Poisoning: A Longitudinal Diffusional Kurtosis Imaging Study

Y. Zhang, T. Wang, J. Lei, S. Guo, S. Wang, Y. Gu, S. Wang, Y. Dou, and X. Zhuang

ABSTRACT

BACKGROUND AND PURPOSE: Previous DTI cross-sectional studies have showed the cerebral damage feature was different in the three clinical stages after carbon monoxide poisoning. Diffusional kurtosis imaging (DKI) is an advanced diffusion imaging model and considered to better provide microstructural contrast in comparison with DTI parameters. The primary aim of this study was to assess microstructural changes in gray and white matter with diffusional kurtosis imaging in the acute, delayed neuropsychiatric, and chronic phases after acute carbon monoxide (CO) poisoning. The secondary aim was to relate diffusional kurtosis imaging measures to neuropsychiatric outcomes of acute carbon monoxide poisoning.

MATERIALS AND METHODS: In all, 17 patients with acute carbon monoxide poisoning and 30 sex- and age-matched healthy volunteers were enrolled in the study. Patients were scanned within 1 week, 3–8 weeks, and 6 months after acute carbon monoxide poisoning. Diffusional kurtosis imaging metrics including mean kurtosis, mean diffusivity, fractional anisotropy, and kurtosis fractional anisotropy were measured in 11 ROIs and then further correlated with neuropsychiatric scores.

RESULTS: In WM, mean kurtosis tended to increase from the acute-to-delayed neuropsychiatric phases and then decrease in the chronic phase, while in GM mean kurtosis showed a constant decline. Contrary to mean kurtosis, mean diffusivity first decreased then tended to increase in WM, while in GM, from the acute to chronic phases, mean diffusivity showed a constant increase. In both WM and GM, the fractional anisotropy and kurtosis fractional anisotropy values progressively declined with time. Kurtosis fractional anisotropy showed the best diagnostic efficiency with an area under the curve of 0.812 ($P = .000$). Along with neuropsychiatric scores, kurtosis fractional anisotropy of the centrum semiovale and Digit Span Backward were most relevant ($r = 0.476, P = .000$).

CONCLUSIONS: Longitudinally, microstructural changes were inconsistent in WM and GM with time after acute carbon monoxide poisoning. Diffusional kurtosis imaging metrics provided important complementary information to quantify the damage to cognitive impairment.

ABBREVIATIONS: CS = centrum semiovale; DKI = diffusional kurtosis imaging; DNS = delayed neuropsychiatric; FA = fractional anisotropy; GP = globus pallidus; KFA = kurtosis fractional anisotropy; MD = mean diffusivity; MK = mean kurtosis; CC = corpus callosum

Carbon monoxide (CO) poisoning often results in serious cerebral damage. On the basis of clinical behavior, surviving patients usually present with 3 clinical phases: the acute, delayed neuropsychiatric (DNS), and chronic. In the acute phase, a patient with a definite history of acute CO poisoning presents with acute and transient clinical symptoms. The DNS phase represents recurrent neuropsychiatric symptoms after the apparent resolution of acute symptoms (a lucid interval from 2 to 40 days; mean duration, 22 days). Furthermore, patients in the chronic phase present symptoms from the acute to chronic phases (even after 1 year).[1]

Necrosis in the globus pallidus (GP) and demyelination in the white matter have been described as the principal pathologic findings of brain damage with CO poisoning in previous reports.[1,2] For the past few years, diffusion-weighted imaging and

diffusion tensor imaging have been popular methods of assessing the above changes. The results indicated that the apparent diffusion coefficient and fractional anisotropy (FA) values were highly correlated with neuropsychiatric scores.[3-7]

Diffusional kurtosis imaging (DKI) is a straightforward extension of the DTI model and is considered to better provide microstructural contrast in comparison with DTI parameters.[8,9] DKI has been experimentally demonstrated to be suitable in both WM and gray matter.[10] The kurtosis reveals the degree of diffusion restriction and tissue microstructural complexity.[11] Evidence from previous research supports elevated kurtosis indicating increased cellular microstructural density, such as with cytotoxic edema or the growth of tumor cells. In contrast, decreasing kurtosis in normal aging and degenerative diseases often suggests myelin destruction or cell loss.[12] Previous research has already depicted brain damage by DKI, but this was a cross-sectional study and observed only WM damage.[13] Due to the longitudinal nature of this study, we were able to observe the dynamic characterization of damage. In addition, this study is comprehensive because we chose both the WM and GM as the ROIs.

Among the parameters we chose, mean kurtosis (MK) was the average of the diffusion kurtosis along all diffusion directions, and higher MK indicated increased microstructural complexity. Mean diffusivity (MD) was viewed as a measurement of isotropic diffusion in the context of free movement of water, and a lower MD value indicated cytotoxic edema, while a higher value represented angiogenic edema. FA reflected water diffusion anisotropy along the 3 principal directions; kurtosis fractional anisotropy (KFA) was mathematically analogous to FA but reflected the anisotropy of the kurtosis tensor.[14] Decline in FA and KFA indicated injured WM fiber integrity.

Our hypothesis was that the evolution of MD, MK, FA, and KFA in the ROIs might be dynamic in the 3 clinical periods; thus, the main purpose of this study was to determine whether DKI metrics could be sensitive enough to dynamically detect microstructural injuries of WM and GM after acute CO poisoning and whether this was useful in evaluating cognitive and executive outcomes.

MATERIALS AND METHODS
Patient Enrollment
The Department of Neurology of the First Hospital of Lanzhou University recruited patients with CO exposure from October 2015 to September 2018. Patients were selected using the following criteria: a clear history of recent CO exposure and DNS occurrence at follow-up. The exclusion criteria were as follows: age younger than 20 years or older than 70 years and a history of brain disorders, including traumatic brain injury, neuropsychiatric disorder, an operation, irradiation, stroke, infection, neoplasm, and demyelinating disease. After initial screening, 17 patients were enrolled in this study. The Ethics Committee of The First Hospital of Lanzhou University approved the study program (LDYYLL2018-114).

Baseline scans and cognitive evaluations were performed within 7 days after acute CO poisoning; follow-up scans were performed within 7 days after DNS occurrence and after 6 months of acute CO poisoning.

Thirty sex- and age-matched healthy subjects were enrolled as controls. All of them had normal MR imaging findings and basic blood test results.

Cognitive Testing
Neuropsychological tests were administered by Tianhong Wang (associate chief physician in neurology) before MR imaging on the same day. The Mini-Mental State Examination was used to assess general intellectual function.[15] Executive function assessments included Digit Forward Span and Digit Backward Span. To evaluate verbal fluency, we asked subjects to name as many items as possible from semantic categories (animals and vegetables). The Barthel Index was used to measure biologic and psychosocial functions.[16]

MR Imaging Protocols
All subjects were scanned on a 3T MR imaging system (Magneton Skyra; Siemens, Erlangen, Germany). The sequences and parameters were as follows:

T1-weighted imaging: TR = 1670 ms, TE = 11 ms, FOV = 240×240 mm, 320×224 matrix, and slice thickness = 2.5 mm.
DWI: single-shot echo-planar sequence—TR = 4500 ms, TE = 102 ms, FOV = 240×240 mm, matrix = 192×192, and slice thickness = 2.5 mm. A b-value of 1000 s/mm^2 was chosen.
DKI: spin-echo EPI diffusion sequence with a total of 30 different diffusion-encoding directions. On the basis of previous studies, the b-value in WM should be higher than that in GM, where 2500∼3000 s/mm^2 was found to be ideal in WM.[17,18] Therefore, the b-values of 0, 1000, and 3000 s/mm^2 were used in this scan.

Axial images were acquired using the following parameters: TR = 6000 ms, TE = 96 ms, FOV = 240×240 mm, matrix = 192×192, and section thickness = 2.5 mm.

The baseline and followed-up scans were performed by the same technician (Xin Zhuang), and the same positioning baseline and parameters. Images were corrected for motion and eddy currents using the eddy-correct tool of the FMRIB Software Library (FSL; https://fsl.fmrib.ox.ac.uk/fsl/fslwiki/). DKI postprocessing was performed using the free software Diffusion Kurtosis Estimator (http://www.nitrc.org/projects/dke), which generated parametric maps including FA, MD, MK, and KFA. ROI delineation and measurement were performed on the software MRIcron (https://www.nitrc.org/projects/mricron/).

MD, MK, FA, and KFA Data Analysis
As the vulnerable damage regions and important functional areas,[2,19,20] the GP, caudate nucleus, thalamus, centrum semiovale (CS), corpus callosum (CC), frontal lobe, occipital lobe, temporal lobe, and parietal lobe were chosen as our ROIs. Every ROI was represented by a sphere with a diameter of 3 mm to lessen partial volume effects, and they were manually placed on T1WI (Fig 1)[13-21] and transferred onto the corresponding parametric map. After ensuring the same scan section, we applied the initially defined ROIs to the follow-up maps. Except for the CC genu, body, and splenium, other ROIs were placed bilaterally, and the mean value was extracted.
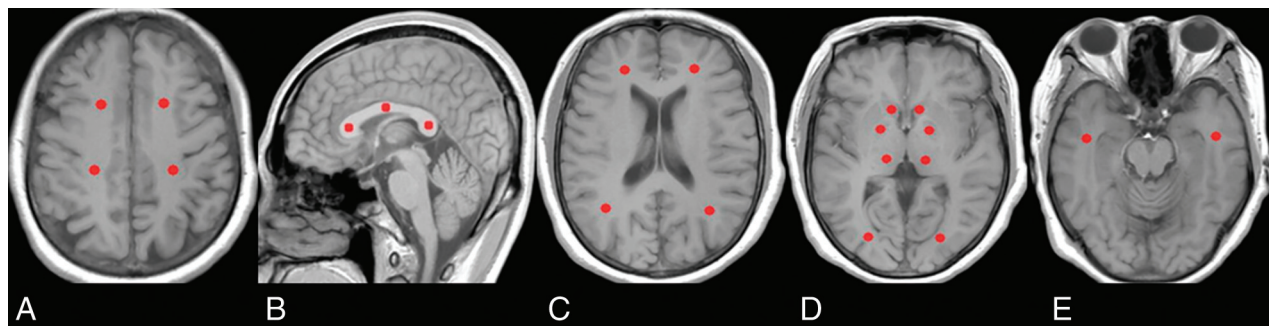
FIG 1. Location of the ROIs. *A*, Centrum semiovale. *B*, Genu, body, and splenium of the corpus callosum. *C*, Frontal and parietal lobes. *D*, Globus pallidus, caudate nucleus, thalamus, and occipital lobe. *E*, Temporal lobe.

Table 1: Clinical variables of patients in different stages of CO exposure[a]

	CO-Exposure Group (n = 17)			
	Acute Stage	**DNS Stage**	**Chronic Stage**	**Controls (n = 30)**
Average days to evaluation	5.53 ± 1.07	30.76 ± 5.90	196.41 ± 9.21	
Sex (male/female) (No.)	8:9	8:9	8:9	15:15
Age (yr)	47.41 ± 11.50	47.41 ± 11.50	47.41 ± 11.50	48.40 ± 9.84
Education (yr)	14.00 (9.50 ± 14.00)	14.00 (9.50 ± 14.00)	14.00 (9.50 ± 14.00)	14.00 (11.00 ± 14.00)
MMSE	26.00 ± 2.50[b,c]	18.59 ± 4.21[c,d]	24.59 ± 2.81[c]	29.00 (28.00–29.00)
Barthel Index	90.00 (80.00–100.00)[b,c]	25.00 (16.00–45.00)[c,d]	98.00 (92.50–100.00)[c]	100.00 (100.00-100.00)
Digit span test				
Forward	6.00 ± 1.46[b,c]	2.00 (1.50–3.00)[c,d]	5.06 ± 1.98[c]	7.00 (7.00–8.00)
Backward	3.76 ± 1.25[b,c]	1.00 (1.00–1.00)[c,d]	2.41 ± 0.94[c]	5.00 (4.00–5.00)
Verbal fluency test				
Animals	11.18 ± 3.36[b,c]	5.47 ± 2.90[c,d]	9.53 ± 3.15[c]	15.00 (14.75.00–16.00)
Vegetables	11.59 ± 2.29[b,c]	5.00 (3.50–6.00)[c,d]	11.00 (9.50–12.00)[c]	13.87 ± 1.50

Note:—MMSE indicates Mini-Mental State Examination.
[a] Data are expressed as mean ± SD and median (25th to 75th quartiles).
[b] $P < .05$ (acute versus DNS).
[c] $P < .05$ (versus controls).
[d] $P < .05$ (DNS versus chronic).

Statistical Analyses

The statistical analysis was performed using the Statistical Package for Social Sciences software package (Version 22 for Windows; IBM, Armonk, New York). The Friedman test and post hoc pair-wise comparisons were used to assess neuropsychiatric scores and DKI parameters of the 3 clinical periods. In post hoc pair-wise comparisons, *P* values adjusted by the Bonferroni correction (the original *P* values multiplied by 3) were compared, with the usual nominal threshold of .05. Two independent-samples *t* tests or Mann-Whitney *U* tests were used to compare the differences between patients and controls. The area under the curve of each DKI parameter in different regions was calculated by receiver operating characteristics. Spearman correlation analysis was used to explore the relationship between the cognitive score and the DKI-derived parameter. *P* values < .05 were considered significant for the tests.

RESULTS
Demographic and Neuropsychiatric Data

Table 1 summarizes the clinical data of the 2 groups. The CO-exposure group had significantly lower neuropsychiatric scores than the control group ($P < .05$). These scores decreased from the acute-to-DNS phases and then increased at the chronic phase ($P < .05$).

Comparisons of DKI-Derived Parameters

The change in DKI metrics is shown in the On-line Table and Fig 2. Compared with the control value, the FA and KFA values of all ROIs showed a decreasing trend in the CO-exposure group. In the CS, corpus callosum body, and corpus callosum splenium, a significant increase in MK and a decrease in MD emerged in the DNS phase. In the GP, however, the highest MK and lowest MD values appeared in the acute phase ($P < .05$).

Among the CO-exposure group, MK in WM showed a trend of increasing from the acute to DNS phases and then decreased at the chronic phase. Contrary to MK, MD first decreased from baseline to the DNS phase and then increased in the chronic phase.

In the GM, from the acute to chronic phase, MK progressively decreased, while MD continually increased. However, in both the WM and GM, the values of FA and KFA showed a trend toward progressive reduction with time.

Comparison of Positive Imaging Characteristics in the 3 Clinical Phases

Figures 3 and 4 represent evolving lesions in the GP and CS, respectively, depicted in the 5 imaging maps in patients 1 and 2 with acute CO poisoning, arranged in the acute, DNS, and chronic phases.
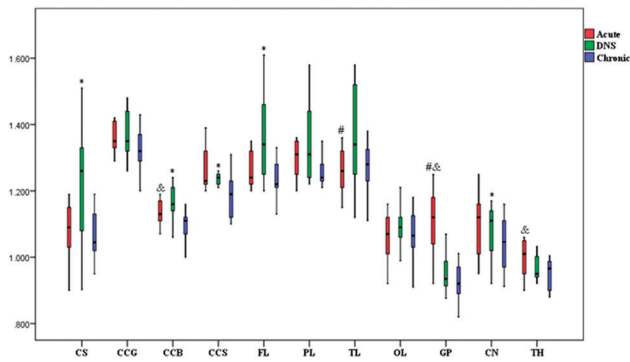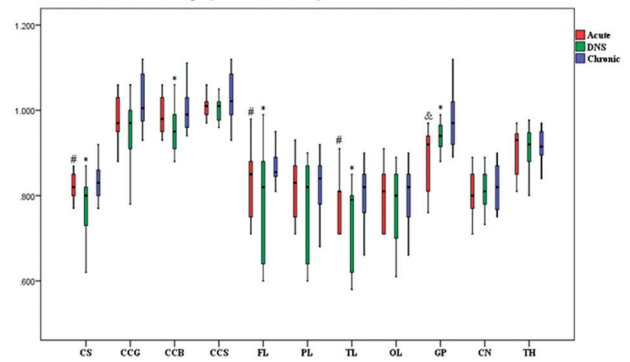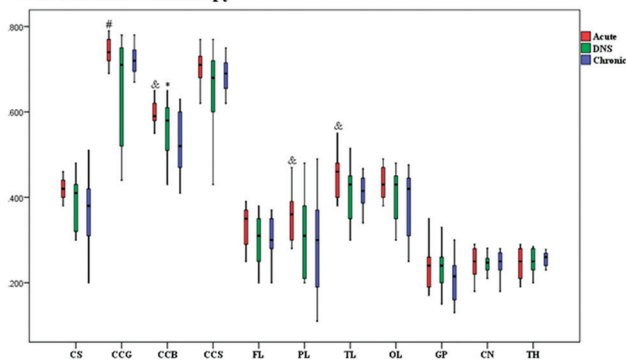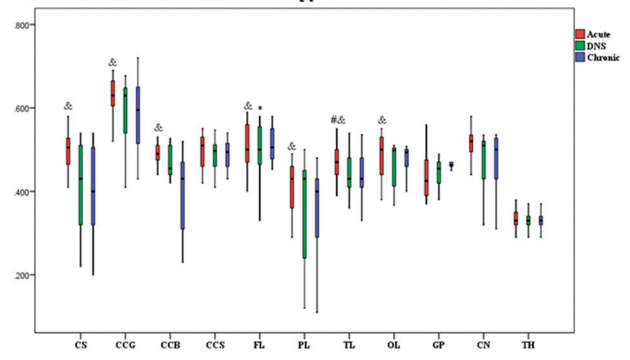
FIG 2. Boxplots of diffusional kurtosis imaging in ROIs in the acute phase (*red bar*), DNS phase (*green bar*), and chronic phase (*blue bar*) with CO intoxication. The *hashtag* indicates $P < .05$ (acute versus DNS); *ampersand*, $P < .05$ (acute versus chronic); and *asterisk*, $P < .05$ (DNS versus chronic).
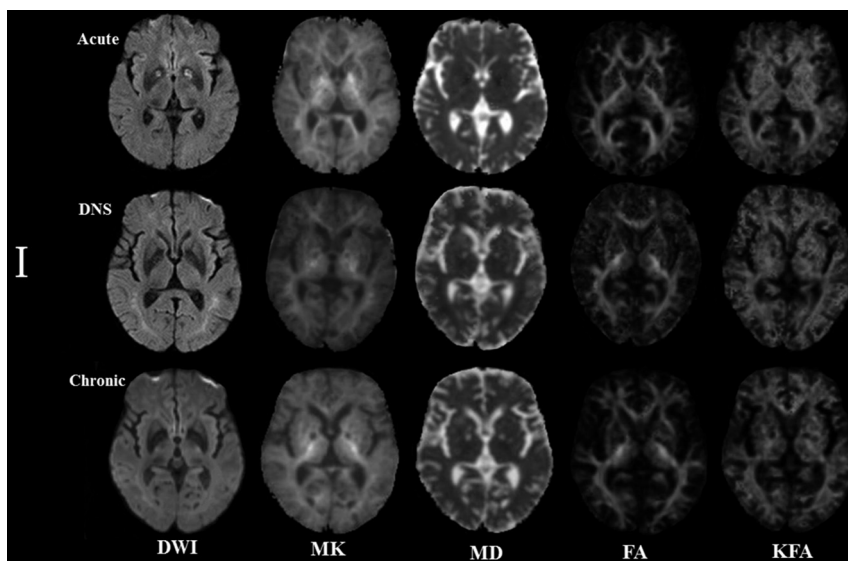
FIG 3. Patient 1: A 54-year-old man. The lesion evolution in the globus pallidus in the acute (5 days), delayed neuropsychiatric (39 days), and chronic (192 days) phases.

In patient 1, symmetric hyperintense lesions in the GP on DWI and MK maps in the acute phase were hypointense lesions on other maps. In the DNS phase, the lesions decreased to isointense lesions on DWI, while they were hypointense lesions on MK and hyperintense lesions on MD maps; in the chronic phase, the intensity of lesions was lower than in the DNS phase on MK maps but higher on MD maps. In both the DNS and chronic phases, the lesions on the FA and KFA maps had lower intensity than those in the acute phase. Notably, in the DNS phase, new hyperintensity lesions emerged in the WM.

In patient 2, slightly hyperintense lesions appeared in the CS in the acute phase on the DWI and MK maps but were isointense lesions on other maps. In the DNS phase, they were higher on the DWI and MK maps and were hypointense lesions on the MD, FA, and KFA maps. In the chronic phase, the intensity significantly decreased on the MK map but increased on the MD map, yet the lesions were still hypointense on the FA and KFA maps.

Diagnostic Performance of DKI-Derived Parameters

In the WM region, KFA had a higher area under the curve than the other measures, among which KFA in the CS had the best performance to differentiate patients in the DNS phase from controls with an area under the curve of 0.812 ($P = .000$) (Table 2). Unlike WM, in the GM region, MK had better differentiation performance than other measures.

KFA Value Predicted Cognitive Performance

The correlations between KFA in the selected ROIs and neuro-psychiatric scores are shown in Table 3. The results show that reduction in KFA in the CS, corpus callosum genu, corpus callosum splenium, frontal lobe, parietal lobe, and GP was significantly associated with a decline in the Mini-Mental State Examination scores ($P < .05$). A decline in the Digit Span Backward score was associated with a KFA decrease in the CS, corpus callosum genu, corpus callosum body, corpus callosum splenium, frontal lobe, parietal lobe, and GP ($P < .05$). However, the Barthel Index, Digit Span Forward, and verbal fluency scores had a slight correlation with all regions.

DISCUSSION

Dynamic Changes in the MK and MD

Physiopathologic changes induced by hypoxic-ischemic damage with CO poisoning included mainly intracellular tortuosity and viscosity changes, which were subsequent to the breakdown of cytoskeletal structures and swelling of the mitochondria, and augmented the complexity or heterogeneity of the microenvironment, eventually leading to an increase in MK. Meanwhile, the cytotoxic edema reduced the extracellular volume and restriction in water motion, which gave rise to a decrease in MD. Our results showed that the change in MK was always contrary to that in MD, both in WM and GM. Accompanied by cell necrosis, liquefaction, apoptosis, and atrophy, the complexity of the tissue appeared to significantly decrease and the vasogenic edema increased. The former resulted in a decrease in MK,[22] and the latter resulted in the increase in MD.

Notably, our results show that increasing MK and decreasing MD appeared earlier in GM than in WM. This finding might be attributed to the increased vulnerability to hypoxia of GM because neurons in GM have high blood demand. In addition, it also indicates that obvious damage in WM occurred in the DNS phase. As we observed, all patients had typical bilateral hyperintensity of WM on DWI in the DNS phase, while in the acute phase, only 5 patients had multiple focal lesions in the WM. These findings were consistent with previous research showing that hyperintense areas in WM on T2-weighted imaging were more widespread after the appearance of the DNS phase than before it.[23,24]

In a previous report, the kurtosis values in the WM region were lower in patients than in controls.[13] However, our results showed that MK was higher in the acute and DNS stages in the CO-exposure group than in the control group; this finding indicates the increased microstructural complexity in the early stages of poisoning. In fact, an increase of MK also occurred in acute stroke research. Jensen et al[25] found
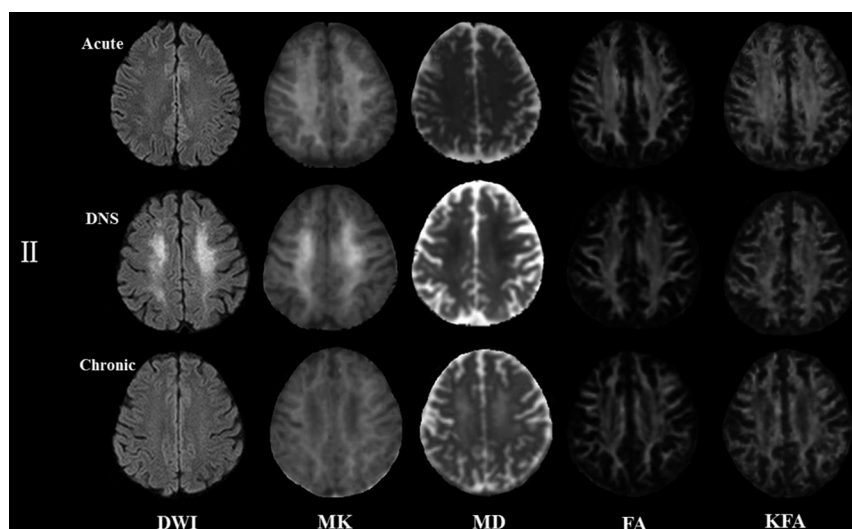

FIG 4. Patient 2: A 42-year-old woman. The lesion evolution in the centrum semiovale in the acute (4 days), delayed neuropsychiatric (25 days), and chronic (223 days) phases.

Table 2: Diagnostic performance of DKI parameters in differentiating patients with CO exposure from controls

Brain Regions/ROIs	Acute Stage				DNS Stage				Chronic Stage			
	MK	MD	FA	KFA	MK	MD	FA	KFA	MK	MD	FA	KFA
White matter												
Centrum semiovale	0.588[a]	0.549	0.555	0.667	0.774[a]	0.770[a]	0.667	0.812[a]	0.516	0.521	0.732[a]	0.802[a]
Corpus callosum												
Genu	0.126	0.522	0.499	0.701[a]	0.599	0.642	0.700[a]	0.753[a]	0.574	0.663[a]	0.681[a]	0.766[a]
Body	0.618	0.601	0.570	0.602	0.759[a]	0.714[a]	0.699[a]	0.780[a]	0.649	0.586	0.789[a]	0.810
Splenium	0.578	0.719[a]	0.600	0.749[a]	0.674	0.768	0.707[a]	0.770[a]	0.720[a]	0.416	0.729[a]	0.811[a]
Frontal	0.651	0.564	0.602	0.671	0.726[a]	0.640	0.736[a]	0.741[a]	0.503	0.612	0.757[a]	0.771[a]
Parietal	0.532	0.583	0.557	0.646	0.637	0.639	0.656	0.697[a]	0.605	0.429	0.697[a]	0.762[a]
Temporal	0.567	0.622	0.575	0.731[a]	0.671	0.745[a]	0.749[a]	0.806[a]	0.604	0.509	0.699	0.775[a]
Occipital	0.645	0.515	0.671	0.693	0.701[a]	0.609	0.733[a]	0.775[a]	0.287[a]	0.503	0.761[a]	0.791[a]
Gray matter												
Globus pallidus	0.800[a]	0.76[a]	0.541	0.633	0.649	0.448	0.553	0.541	0.724[a]	0.640	0.660	0.602
Caudate nucleus	0.562	0.516	0.520	0.501	0.539	0.514	0.551	0.514	0.659[a]	0.535	0.603	0.613
Thalamus	0.590	0.585	0.556	0.477	0.550	0.379	0.509	0.520	0.700[a]	0.400	0.534	0.537

Note:—ROC indicates receiver operating characteristic.

[a] <.05 indicates significance.

Table 3: Correlation study between KFA and cognitive tests in patients with CO intoxication

| Brain Regions/ROIs | MMSE | Barthel Index | Digit Span | | Verbal Fluency | |
			Forward	Backward	Animals	Vegetables
White matter						
Centrum semiovale	r = 0.399[a]	r = 0.125	r = 0.212	r = 0.476[a]	r = 0.164	r = 0.221[a]
	P = .000	P = .268	P = .057	P = .000	P = .145	P = .048
Corpus callosum						
Genu	r = 0.283[a]	r = 0.141	r = 0.218	r = 0.374[a]	r = 0.167	r = 0.188
	P = .010	P = .209	P = .051	P = .001	P = .136	P = .092
Body	r = 0.206	r = 0.211	r = 0.232[a]	r = 0.364[a]	r = 0.219[a]	r = 0.176
	P = .065	P = .059	P = .037	P = .001	P = .049	P = .117
Splenium	r = 0.346[a]	r = 0.252[a]	r = 0.201	r = 0.270[a]	r = 0.200	r = 0.282[a]
	P = .002	P = .023	P = .073	P = .015	P = .073	P = .011
Frontal	r = 0.324[a]	r = 0.155	r = 0.173	r = 0.391[a]	r = 0.203	r = 0.170
	P = .003	P = .167	P = .123	P = .000	P = .069	P = .129
Parietal	r = 0.222[a]	r = 0.122	r = 0.158	r = 0.413[a]	r = 0.141	r = 0.152
	P = .047	P = .279	P = .159	P = .000	P = .211	P = .174
Temporal	r = 0.174	r = 0.171	r = 0.246[a]	r = 0.172	r = 0.091	r = −0.007
	P = .119	P = .127	P = .027	P = .124	P = .417	P = .948
Occipital	r = 0.151	r = 0.115	r = 0.187	r = 0.141	r = 0.142	r = 0.087
	P = .178	P = .305	P = .095	P = .210	P = .208	P = .442
Gray matter						
Globus pallidus	r = 0.282[a]	r = 0.206	r = 0.280[a]	r = 0.264[a]	r = 0.217	r = 0.175
	P = .011	P = .065	P = .011	P = .017	P = .051	P = .119
Caudate nucleus	r = −0.052	r = −0.148	r = −0.185	r = 0.108	r = −0.115	r = −0.118
	P = .645	P = .188	P = .099	P = .338	P = .308	P = .294
Thalamus	r = 0.068	r = 0.039	r = −0.018	r = 0.054	r = 0.111	r = 0.040
	P = .544	P = .726	P = .871	P = .630	P = .323	P = .720

Note:—MMSE indicates Mini-Mental State Examination.
[a] Significant indicated by<.05.

substantially increased diffusional kurtosis within the cerebral ischemic lesions of 3 subjects with stroke 13-26 hours following the onset of symptoms by application of the DKI MR imaging method. In CO poisoning, these similar results might be explained by secondary ischemic injury caused by hypoxia in the early stage.

By comparing the diagnostic efficiency, we found that MK had a higher sensitivity than MD for monitoring GM damage. This was consistent with previous findings with regard to stroke, Alzheimer disease, Parkinson disease, and neoplastic lesions.[26-31] Compared with other deep GM structures such as the caudate nucleus and thalamus, the GP showed the greatest sensitivity, therefore revealing selective damage to the GP.

Progressive Decrease in FA and KFA

Our results show that FA and KFA of WM progressively decreased with time, which was a finding reported in a previous study: Lo et al[6] reported that a significantly lower mean FA value was found in patients in the DNS phase compared with the control group both before and 3 months after hyperbaric oxygen therapy. Chang et al[32] reported on 17 patients with CO poisoning who underwent DTI assessment 4–6 months after hyperbaric oxygen therapy, and they found that the extensive WM areas with FA decreased. The breakdown of myelin and nerve fiber rarefaction may be an important component of the pathologic process.[14] In addition, we found that the decreases in FA and KFA were more obvious in the DNS and chronic phases than in the acute phase. The underlying mechanisms might be related to neuronal injury that was originally caused by global brain anoxia or

ischemia in the acute phase and then resulted in secondary Wallerian degeneration of WM.[33]

In terms of diagnostic efficiency, KFA showed a better efficiency than FA in detecting WM damage. Indeed, previous reports have demonstrated that KFA supplements the contrast in other diffusion MR imaging metrics, particularly FA, which vanishes in near-orthogonal fiber arrangements such as in the superior corona radiata and centrum semiovale, whereas KFA does not.[13,34]

KFA Value Predicted Clinical Performance

Cognitive and executive capacity dysfunction was the common clinical issue for survivors of CO poisoning. Recently, a study based on a total of 9041 adults showed that the dementia incidence was 1.6-fold higher in the CO-exposed cohort than in the nonexposed cohort.[35] Neuropsychiatric deficits related to CO poisoning were also found in our patients. In our study, the positive correlation between the neuropsychiatric score and KFA in multiple WM regions supported the hypothesis that WM microstructural changes may contribute to the decline in cognitive and executive functions. In fact, there were 5 patients in our study who still had poor neuropsychiatric performance regarding incapacity of life, disturbance of intelligence, or hemiplegic paralysis at the chronic stage and had much lower KFA values (0.102∼0.303) in the CS than others.

Relative to other scores, Digit Span Backward was found to have better correlation with most regions in WM, such as the CS, corpus callosum genu, corpus callosum body, frontal lobe, and parietal lobe. This finding might be because the performance on Digit Span Backward is thought to reflect higher-order executive

abilities.[36] Anatomically, the CS is adjacent to the CC, which consists of large projection fibers such as the corticospinal, corticobulbar, and corticopontine tracts. These large projection fibers widely connect the cerebral cortex of the frontal lobe and parietal lobe regions, mediating mainly executive functions.[37]

In addition, due to the GP being related to the extrapyramidal tract, damage usually caused abnormalities in motor function, eventually leading to a decrease in executive capacity.[38] In our study, 6 patients emerged with Parkinson's symptoms which all occurred in the DNS stage.

Last, with respect to the correlation among levels of CO exposure, neuropsychiatric scores, and DKI metrics, previous studies have shown that there is no definite relationship among carboxyhemoglobin levels, the severity of MR imaging findings, and the length of exposure time.[39]

Limitations
First, DKI metrics were measured on the basis of ROIs manually placed in various regions, which might yield imperfect reference values and were thus biased. Second, only limited neuropsychological tests were performed, possibly underestimating the cognitive sequelae.

CONCLUSIONS
We confirmed our initial hypothesis that the evolution of brain damage with CO intoxication was dynamic across time. WM and GM responses to CO exposure might not be identical. KFA could be a surrogate biomarker for tissue damage and reflected the performance of cognitive and executive functions correlated with prognosis.

REFERENCES

1. Beppu T. **The role of MR imaging in assessment of brain damage from carbon monoxide poisoning: a review of the literature.** *AJNR Am J Neuroradiol* 2014;35:625–31 CrossRef Medline
2. Jeon SB, Sohn CH, Seo DW, et al. **Acute brain lesions on magnetic resonance imaging and delayed neurological sequelae in carbon monoxide poisoning.** *JAMA Neurol* 2018;75:436–43 CrossRef Medline
3. Chen NC, Huang CW, Lui CC, et al. **Diffusion-weighted imaging improves prediction in cognitive outcome and clinical phases in patients with carbon monoxide intoxication.** *Neuroradiology* 2013;55:107–15 CrossRef Medline
4. Fujiwara S, Beppu T, Nishimoto H, et al. **Detecting damaged regions of cerebral white matter in the subacute phase after carbon monoxide poisoning using voxel-based analysis with diffusion tensor imaging.** *Neuroradiology* 2012;54:681–89 CrossRef Medline
5. Lin WC, Lu CH, Lee YC, et al. **White matter damage in carbon monoxide intoxication assessed in vivo using diffusion tensor MR imaging.** *AJNR Am J Neuroradiol* 2009;30:1248–55 CrossRef Medline
6. Lo CP, Chen SY, Chou MC, et al. **Diffusion-tensor MR imaging for evaluation of the efficacy of hyperbaric oxygen therapy in patients with delayed neuropsychiatric syndrome caused by carbon monoxide inhalation.** *Eur J Neurol* 2007;14:777–82 CrossRef Medline
7. Terajima K, Igarashi H, Hirose M, et al. **Serial assessments of delayed encephalopathy after carbon monoxide poisoning using magnetic resonance spectroscopy and diffusion tensor imaging on 3.0T system.** *Eur Neurol* 2008;59:55–61 CrossRef Medline
8. Lu H, Jensen JH, Ramania, et al. **Three-dimensional characterization of non-Gaussian water diffusion in humans using diffusion kurtosis imaging.** *NMR Biomed* 2006;19:236–47 CrossRef Medline
9. Jensen JH, Helpern JA. **MRI quantification of non-Gaussian water diffusion by of non-Gaussian water diffusion by analysis.** *NMR Biomed* 2010;23:698–10 CrossRef Medline
10. Assaf Y, Cohen Y. **Non-mono-exponential attenuation of water and N-acetyl aspartate signals due to diffusion in brain tissue.** *J Magn Reson* 1998;131:69–85 CrossRef Medline
11. Lazar M, Jensen JH, Xuan L, et al. **Estimation of the orientation distribution function from diffusional kurtosis imaging.** *Magn Reson Med* 2008;60:774–81 CrossRef Medline
12. Marrale M, Collura G, Brai M, et al. **Physics-techniques and review of neuroradiological applications of diffusion kurtosis imaging (DKI).** *Clin Neuroradiol* 2016;26:391–03 CrossRef Medline
13. Lee JJ, Chang WN, Hsu JL, et al. **Diffusion kurtosis imaging as a neuroimaging biomarker in patients with carbon monoxide intoxication.** *Neurotoxicology* 2018;68:38–46 CrossRef Medline
14. Hansen B, Jespersen SN. **Kurtosis fractional anisotropy: its contrast and estimation by proxy.** *Sci Rep* 2016;6:23999 CrossRef Medline
15. Folstein MF, Folstein SE, McHugh PR. **Mini-mental state: a practical method for grading the cognitive state of patients for the clinician.** *J Psychiatr Res* 1975;12:189–98 CrossRef Medline
16. Sidney K, Amasa BF, Roland WM, et al. **Studies of illness in the aged. The index of ADL: a standardized measure of biological and psychosocial function.** *JAMA* 1963;185:914–19 CrossRef Medline
17. Chuhutin A, Hansen B, Jespersen SN. **Precision and accuracy of diffusion kurtosis estimation and the influence of b-value selection.** *NMR Biomed* 2017;30 CrossRef Medline
18. Hansen B, Jespersen SN. **Recent developments in fast kurtosis imaging.** *Front Phys* 2017;5:1–15 CrossRef
19. Barha CK, Nagamatsu LS, Liu-Ambrose T. **Basics of neuroanatomy and neurophysiology.** *Handb Clin Neurol* 2016;138:53–68 CrossRef Medline
20. Schmahmann JD, Smith EE, Eichler FS, et al. **Cerebral white matter: neuroanatomy- clinical neurology-and neurobehavioral correlates.** *Ann N Y Acad Sci* 2008;1142:266–09 CrossRef Medline
21. Kanda T, Ishii K, Kawaguchi H, et al. **High signal intensity in the dentate nucleus and globus pallidus on unenhanced T1-weighted MR images: relationship with increasing cumulative dose ofa gadolinium-based contrast material.** *Radiology* 2014;270:834–41 CrossRef Medline
22. Coutu JP, Chen JJ, Rosas HD, et al. **Non-Gaussian water diffusion in aging white matter.** *Neurobiol Aging* 2014;35:1412–21 CrossRef Medline
23. Inagaki T, Ishino H, Seno H, et al. **A long-term follow-up study of serial magnetic resonance images in patients with delayed encephalopathy after acute carbon monoxide poisoning.** *Psychiatry Clin Neurosci* 1997;51:421–23 CrossRef Medline
24. Vila JF, Meli FJ, Serqueira OE, et al. **Diffusion tensor magnetic resonance imaging: a promising technique to characterize and track delayed encephalopathy after acute carbon monoxide poisoning.** *Undersea Hyperb Med* 2005;32:151–56 Medline
25. Jensen JH, Falangola MF, Hu C, et al. **Preliminary observations of increased diffusional kurtosis in human brain following recent cerebral infarction.** *NMR Biomed* 2011;24:452–57 CrossRef Medline
26. Hui ES, Fieremans E, Jensen JH, et al. **Stroke assessment with diffusional kurtosis imaging.** *Stroke* 2012;43:2968–73 CrossRef Medline
27. Falangola MF, Jensen JH, Tabesha, et al. **Non-Gaussian diffusion MRI assessment of brain microstructure in mild cognitive impairment and Alzheimer's disease.** *Magn Reson Imaging* 2013;31:840–46 CrossRef Medline
28. Kamagata K, Tomiyama H, Motoi Y, et al. **Diffusional kurtosis imaging of cingulate fibers in Parkinson disease: comparison with conventional diffusion tensor imaging.** *Magn Reson Imaging* 2013;31:1501–06 CrossRef Medline

29. Wang JJ, Lin WY, Lu CS, et al. **Parkinson disease: diagnostic utility of diffusion kurtosis imaging.** *Radiology* 2011;261:210–17 CrossRef Medline

30. Van Cauter S, Veraart J, Sijbers J, et al. **Gliomas: diffusion kurtosis MR imaging in grading.** *Radiology* 2012;263:492–01 CrossRef Medline

31. Cheung JS, Wang E, Lo EH, et al. **Stratification of heterogeneous diffusion MRI ischemic lesion with kurtosis imaging: evaluation of mean diffusion and kurtosis MRI mismatch in an animal model of transient focal ischemia.** *Stroke* 2012;43:2252–54 CrossRef Medline

32. Chang CC, Lee YC, Chang WN, et al. **Damage of white matter tract correlated with neuropsychological deficits in carbon monoxide intoxication after hyperbaric oxygen.** *J Neurotrauma* 2009;26:1263–70 CrossRef Medline

33. Bartzokis G. **Age-related myelin break down: a developmental model of cognitive decline and Alzheimer's disease.** *Neurobiol Aging* 2004;25:5–18 CrossRef Medline

34. Pantoni L, Garcia JH, Gutierrez JA. **Cerebral white matter is highly vulnerable to ischemia.** *Stroke* 1996;27:1641–46 Medline

35. Lai CY, Huang YW, Tseng CH, et al. **Patients with carbon monoxide poisoning and subsequent dementia: a population-based cohort study.** *Medicine (Baltimore)* 2016;95:e2418. CrossRef Medline

36. O'Donnell JP, MacGregor LA, Dabrowski JJ, et al. **Construct validity of neuropsychological tests of conceptual and attentional abilities.** *J Clin Psychol* 1994;50:596–600 CrossRef Medline

37. Baddeley A, Della Sala S. **Working memory and executive control.** *Philos Trans R Soc Lond B Biol Sci* 1996;351:1397–03 CrossRef Medline

38. Saga Y, Hoshi E, Tremblay L. **Roles of multiple globus pallidus territories of monkey and humans in motivation, cognition and action: an anatomical, physiological and pathophysiological review.** *Front Neuroanat* 2017;10;11 CrossRef

39. Kim DM, Lee IH, Park JY, et al. **Acute carbon monoxide poisoning: MR imaging findings with clinical correlation.** *Diagn Interv Imaging* 2017;98:299–06 CrossRef Medline